Chapter 4
Measurements of Hardness and Other Mechanical Properties of Hard and Superhard Materials and Coatings

Dr. Maritza G.J. Veprek-Heijman
and Prof. Dr. Prof. h.c. Dr. h.c. Stan Veprek

Abstract We discuss the methods and problems associated with a reliable measurements of mechanical properties of superhard ($H \geq 40$ GPa) and ultrahard ($H \geq 80$ GPa) materials and coatings. It is shown that the "nanoindentation" can yield incorrect results of hardness and elastic moduli when applied to super- and ultrahard materials. Therefore, the classical two-step method, where, after the indentation with a given load, the size of remnant indentation is measured by a microscope, is recommended for the verification of the results obtained from the "nanoindentation." We further discuss methods for the determination of elastic moduli, tensile yield strength, and internal friction. Special attention is devoted to the measurement of the mechanical properties of super- and ultrahard thin films on softer substrates. It is shown that the Bückle's rule, according to which the indentation depth should not exceed 10 % of the film thickness of a hard film on soft substrate, does not apply for hard and superhard materials.

1 Introduction

Experimental determination of the mechanical properties of hard and superhard materials is usually not an easy task. In many cases, a large load of several newtons (N) has to be applied during the hardness measurement to achieve the load-invariant value of the hardness. Also the compliance of the testing systems used may be higher than that of the sample being tested. This makes the accurate determination

Dr. M.G.J. Veprek-Heijman (✉)
Department of Chemistry, Technical University Munich, Munich, Germany
e-mail: Maritza.Veprekheijman@lrz.tum.de

Prof. Dr. Prof. h.c. Dr. h.c. S. Veprek
Professor Emeritus, Department of Chemistry, Technical University Munich, Munich, Germany
e-mail: Stan.Veprek@lrz.tum.de

V. Kanyanta (ed.), *Microstructure-Property Correlations for Hard, Superhard, and Ultrahard Materials*, DOI 10.1007/978-3-319-29291-5_4

of the deformations in the sample very difficult, particularly when using the modern automated load-depth sensing techniques with instruments called "nanoindentometers." The properties of the materials are often affected by the residual stress in the structure due to the manufacturing route used. This is particularly important for hard and superhard coatings on softer substrates. These and other issues, challenges, and methods of overcoming them will be discussed in this chapter with focus on the correct measurements of hardness of bulk materials as well as of thin films on softer substrates and wear protection coatings on tools for machining. Because the measurements of fracture toughness, which is also an important property of hard (hardness $H \geq 10$ GPa), superhard ($H \geq 40$ GPa), and ultrahard ($H \geq 80$ GPa) materials, will be discussed in Chap. 5, we limit our discussion of this topic only to a short remark. Also the coefficient of friction, μ, will be mentioned only briefly. Special attention is devoted to the measurement of elastic moduli, yield strength, and the thickness of the hard, superhard, and ultrahard thin films on softer substrate that is needed for correct measurement. It is shown that for the correct hardness measurements, the required thickness of the hard, superhard, and ultrahard thin film on a soft substrate must be much larger than what the Bückle's rule of 10 % suggests.

The fracture toughness, expressed in terms of stress intensity factor K_I given by Eq. 4.1 (here, σ is the stress needed to propagate a crack of a size $2a$, and *Const*. is a factor that takes into account the flaw shape and geometry, as well as the loading mode configuration (Anderson 1995)), is the resistance of a material against the propagation of a preexisting (prefabricated) crack (McClintock and Argon 1966; Hertzberg 1989; Anderson 1995). It should be emphasized that one has to distinguish between fracture toughness defined in this way and the resistance against brittle fracture due to the absence of microcracks and other flaws in the material because of a high-threshold limit needed to initiate a crack in an optimally processed material. This can be easily understood by comparing the Griffith formula for critical stress σ_C needed for propagation of a penny-shaped crack of diameter $2a$ given in Eq. 4.2 (here, E_Y is the Young's modulus and γ_C is the surface energy) and the ideal decohesion strength σ_{Decoh} given by Eq. 4.3 (here a_0 is the interatomic distance; Kelly and Macmillan 1986).

$$K_I = \text{Const.} \cdot \sigma \cdot \sqrt{\pi \cdot a} \tag{4.1}$$

$$\sigma_C = \sqrt{\frac{2E_Y \cdot \gamma_S}{\pi \cdot a}} \tag{4.2}$$

$$\sigma_{\text{Decoh.}} = \sqrt{\frac{2E_Y \cdot \gamma_S}{\pi \cdot a_0}} \tag{4.3}$$

In an optimally processed polycrystalline material, the size of cracks resulting from the preparation scales approximately with the crystallite size d. Therefore, σ_C is relatively small in coarse-grained polycrystalline materials where a is of the order of tens microns, but it strongly increases for nanocrystalline materials where it can approach the ideal decohesion strength σ_{Decoh} (Veprek et al. 1996; Veprek 1999).

Such material can reach a high elastic limit of several percentage or more approaching that of an ideal flaw-free material (Veprek and Argon 2002; Veprek et al. 2003b). We shall discuss this point in Chap. 6. Whereas the measurement of the fracture toughness (Eq. 4.1) of bulk materials is well established and described in Chap. 5 and in a number of textbooks, the measurement of the threshold for the crack initiation is difficult because it depends on the statistics of the flaws formed during the preparation of the material. The statistical modeling and the probability of the cleavage fracture are calculated either by the relatively simple "weakest link" model or by the truncated Weibull distribution described, e.g., in Anderson (1995) to which we refer for further details.

The coefficient of friction, μ, of a material in a sliding contact with another one describes important property for many applications. It is the force F necessary to keep two surfaces, which are pressed together by a load L_N normal to the direction of the sliding, from sliding against each other (Feynman et al. 1966, p. 12–3 ff.).

$$F = \mu \cdot L_N \tag{4.4}$$

Thus, μ is a dimensionless scalar. The coefficient of friction depends on the asperities of the sliding surfaces, on the surface energy of the materials sliding against each other, on the sliding speed, and on humidity or other environmental effects which can act as lubricants (Bayer 2002). To initiate sliding between two surfaces which are in rest requires higher force F_0 than that in steady-state sliding conditions because the surface asperities are "locked in" at rest (F_0 is called "stiction"). For these and many other reasons, the coefficient of friction has to be measured under precisely defined conditions. Such conditions are usually specified in the user's manuals of tribometers on the market.

Friction may also be important during the measurement of the hardness of materials, because high friction coefficient between the indenter and the sample being measured may result in a falsified, apparently higher, hardness (Tabor 1951). However, because only diamond indenters are used for measuring the hardness of super- and ultrahard materials, and because diamond has a small coefficient of friction of about 0.1 toward the majority of materials (Tabor 1951), this effect is probably not too important. Nevertheless, it should be kept in mind and checked by comparing the value of the hardness measured without and with a lubricant. Friction may also be important when measuring "hot hardness," i.e., hardness at elevated temperature.

One of the important fields of application of super- and ultrahard materials is the machining of metallic alloys, wood, and ceramics. For these applications, bulk materials (c-BN, diamond, cermets) as well as wear protection coatings on tools made of high-speed steel (HSS) or cemented carbide (WC-Co) are used. Important are not only the high hardness, high fracture toughness, and low coefficient of friction, but also high oxidation and chemical resistance against the material being machined. For example, in spite of its high hardness of 70–100 GPa, diamond cannot be used for the machining of ferrous alloys or other materials which contain elements that form stable carbides, because in that case the chemical wear

dominates. Thus, not only purely "mechanical" properties are important in the applications. But these aspects are beyond the scope of this chapter. Therefore, here we shall focus on the measurement of the hardness and afterward discuss the measurements of elastic moduli and some other properties.

2 Hardness

2.1 The Meaning of Hardness

In general sense, hardness is the resistance of a material against plastic deformation under the applied load. Thus, the nature of the applied load defines different hardnesses, such as scratch hardness according to Mohs, impact hardness, or indentation hardness (Tabor 1951). Scratch hardness, being used by mineralogists because of its simplicity, particularly when working in the field, is not suitable for material scientists and engineers because it is strongly nonlinear (see, e.g., McClintock and Argon 1966, p. 450). The dynamic impact hardness is important, e.g., in interrupted cutting, such as milling, for the lacquer on the front part of a vehicle exposed to impact of particles and the like. Because these materials are not superhard, we shall not discuss the impact hardness in any further details here. The definition of the impact hardness can be found in the book by Tabor (1951), and the more recent method of its testing is described by McClintock and Argon (1966), Knotek et al. (1992), and Bouzakis et al. (2007).

From the scientific point of view, most important is the indentation hardness with self-similar indenters, such as Vickers or other pyramidal or conical indenters, where the contact area between the indenter and the material being measured, A_C, is proportional to the square of the indentation depth, h^2. The indentation hardness is the average pressure beneath the indenter under the conditions of fully developed plasticity (Meyer 1908; Tabor 1951). Note that the pressure beneath the indenter is distributed very inhomogenously (see, e.g., Fig. 11 in Veprek et al. 2007). The correctly measured indentation hardness must be load invariant. Unfortunately, this condition is often neglected in many published papers which incorrectly report on "superhard materials" because the measurements have been done at a too small load, where the indentation size effect (ISE, see below) may falsify the hardness measurement (see Veprek-Heijman and Veprek (2015) and references therein).

2.2 Indentation Hardness

The most popular and reliable method of the hardness measured using the self-similar indenters has been the two-step indentation procedure with the Vickers indenter, which is a four-faced pyramid made of diamond with an angle of 136°

between the opposite faces. This angle has been chosen to make the Vickers hardness similar to the Brinell hardness as to yield the same values of hardness. Brinell hardness test uses a spherical indenter which is not self-similar, i.e., the indentation depth or the contact radius has to be specified (Tabor 1951, p. 98). The indenter is pressed into the material being tested with a given load, L, this load is applied for a defined period in order to check for possible creep. After unloading the projected area, A_P, of the remnant plastically deformed indent is measured with a microscope. The contact area, A_C, can be calculated from A_P using the known geometry of the Vickers indenter. Alternatively, the diagonal of the remnant indent is measured and A_C calculated. The Vickers hardness is

$$H_V = L/A_C. \tag{4.5}$$

The engineers use the so-called Vickers number in the units g/mm^2. We shall adhere to the units GPa (10,000 VH $\approx$ 10 GPa). One can also use the projected area of the indent, A_P, which yields the Meyers hardness $H_{Meyer} = L/A_P$. The Vickers and Meyers hardness are related by $H_V = 0.927 \cdot H_{Meyer}$ (Tabor 1951, p. 98), provided the indenter has a sharp tip or the indentation depth is sufficiently large so that the error of h due to the tip rounding can be neglected. It has to be kept in mind that when indenting into superhard materials, the sharp diamond tip is plastically (irreversibly) deformed up to a "radius" 0.5–0.7 μm (see below). Keeping the load applied for a sufficiently long time is necessary when the material being tested undergoes creep under the load.

For an ideal Vickers indenter, the contact area, A_C, and indentation depth, h, are related by Eq. 4.3. However, when the indenter tip is dull, the actual contact area is—for the same indentation depth—larger than that corresponding to Eq. 4.3. Neglecting this "tip rounding" results in incorrect, too high hardness value. This error can be neglected when the indentation depth is large, but it becomes serious when the indentation depth is about 100 nm or less, as is the case with the modern "nanoindentometers."

$$A_C = 26.43h^2 \tag{4.6}$$

Later on, the Berkovich indenter with three faces and cube-corner indenter with four faces have been introduced because they develop larger stress under the sharp tip to assure yielding of the material being tested at a low applied load. The relation between the indentation depth and contact area is similar to Eq. 4.3 with different proportionality constants that can be found, e.g., in Fischer-Cripps (2004). The larger stress that develops under the sharper indenter tips of Berkovich and cube-corner indenters is an important advantage when measuring the hardness of thin films using the automated load–depth-sensing technique called "nanoindentation," which has been introduced by Doerner and Nix (1986) and later on improved by Oliver and Pharr (1992, 2004).

However, the advantage of Berkovich and cube-corner indenters is less pronounced when measuring super- and ultrahard materials because, in that case, the

initially sharp indenter tip undergoes plastic deformation and rounding, as shown by experiment (see Fig. 8 in Veprek et al. 2003a) and by nonlinear finite element modeling (see Figs. 1 and 2 in Veprek-Heijman et al. 2009). Typically, a sharp indenter with a tip "radius"[1] of ≤ 0.1 μm is plastically deformed when indenting into a super- and ultrahard material so that after 2–3 indentations, the "radius" increases to about 0.3–0.5 μm. However, with increasing number of the subsequent indentations, the incremental increase of the tip "radius" is diminishing until it stabilizes at about 0.5–0.7 μm (Fig. 2 in Veprek-Heijman et al. 2009). Upon further indentations, the tip "radius" deforms mainly elastically.

For these reasons, hardness of super- and ultrahard materials can be reproducibly measured only with a dull indenter. This often (but not always, see below and Chap. 6) requires the use of large indentation depth of ≥ 400–600 nm and corresponding large load of up to several N. Such high loads cannot be provided by the majority of the modern "nanoindentometers." Therefore, one has to use the conventional two-step techniques.

As we shall discuss later, the measured apparent hardness increases when the applied load decreases under a certain value (Sect. 2.3). This so-called indentation size effect (ISE) can have a variety of origins, the not perfectly shaped and sharp indenter being only one of them. The ISE due to tip rounding has to be experimentally corrected for by a special procedure called "tip area correction" when using the automated load–depth-sensing technique ("nanoindentation"), which typically uses relatively small load. The early method of Doerner and Nix used the constant hardness method, where the apparent hardness of a reference material is measured as function of applied load up to sufficiently large load where ISE vanishes because the indentation depth is much larger than the error of the indentation depth due to the dull tip, and the correct hardness is measured. Then, a polynomial function is used to transform the measured dependence of the apparent hardness on the applied load as to obtain correct hardness for all points measured at different loads. In the method of Doerner and Nix, about 25 % of the initial part of the unloading indentation curve is linearly extrapolated to zero load, where the so-called corrected indentation depth, h_{Corr}, is obtained. From this value of h_{Corr}, the hardness is calculated according to Eq. 4.2. This procedure is a purely empirical calibration of the instrument, and the value of h_{Corr} is not any real indentation depth (Behncke 1993, Sect. 4.4).[2] Nevertheless, it can provide correct results when the calibration is carefully done as shown in Fig. 4.1. Figure 4.1a shows an example of repetitive measurement of the hardness of Si and sapphire wafers using the early version of the indentometer Fischerscope H100, which has been on the market several years before the paper of Oliver and Pharr has been published. Therefore, it used the

[1] We write "radius" within quotation marks because the tip is not exactly spherical (see Fig. 1 in Veprek-Heijman et al. (2009)).

[2] Doerner and Nix measured the shape of the diamond indenter using scanning electron microscope and used this for the tip area correction.

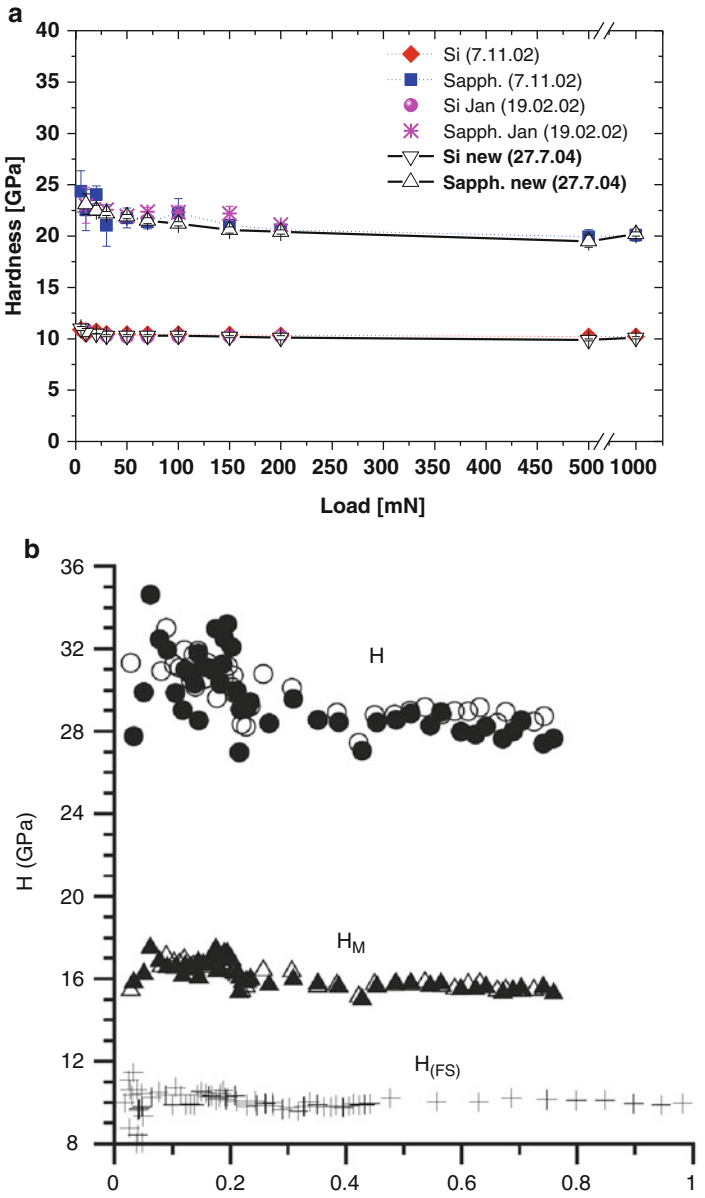

Fig. 4.1 (**a**) Hardness of silicon used for the calibration of the early version of Fischerscope H100 in the constant hardness mode and resultant hardness of sapphire (see also Veprek et al. 2003a). (**b**) Example of the measurement of the hardness, as function of indentation depth, of sapphire using a modern nanoindentometer that has been calibrated according to the Oliver and Pharr procedure using constant stiffness method (see text from Fischer-Cripps et al. 2006)

method of Doerner and Nix [similar results, measured by other coworkers of S. V., have been published in Veprek S et al. (2003a)].

The method of Oliver and Pharr uses for the "tip area correction" constant stiffness method and a power-law fit of the initial part of the unloading curve together with an "intercept factor" to determine the corrected indentation depth (Oliver and Pharr 1992, 2004; Fischer-Cripps 2004). Oliver and Pharr called their procedure "an improved technique for determining hardness. . .," and, after their first paper (Oliver and Pharr 1992), they published several critical papers analyzing possible artifacts which may occur when using this technique (e.g., Oliver and Pharr 2004). Also other researchers analyzed this techniques and suggested many corrections and improvements (e.g., Chaudhri 2001; Chaudhri and Lim 2007; Meza et al. 2007; Rodriguez et al. 2011; Keutenedjian Mady et al. 2012). We cannot review this issue here because the number of the relevant papers is too large. But we would like to emphasize that large care has to be taken when measuring hardness of superhard materials using the "nanoindentation" technique. Unfortunately, the original method of Oliver and Pharr (1992) is often used by the workers without any critical analysis. We would like to illustrate it here by only two examples.

Figure 4.1b shows an example of the hardness of sapphire (see points denoted H) measured with the "nanoindenter" UMIS that has been calibrated by means of the constant stiffness of fused silica using the Oliver and Pharr method (Fischer-Cripps et al. 2006). H_M is the Martens hardness, i.e., the hardness under applied load, H_{FS} is the hardness of the fused silica, and h_C is the corrected indentation depth (h_C of 0.8 μm corresponds to a load of about 200–300 mN). Obviously, the value of the hardness of sapphire obtained by Fischer-Cripps with this method of about 28–30 GPa is too high. There are many papers reporting the hardness of sapphire, measured by the conventional two-step techniques at large load of several N, to be 21 ± 1.5 GPa (e.g., Berg et al. 2000; Müller 1984; Holleck 1986; Kollenberg 1988, homepages of industrial companies producing sapphire such as Kyocera (2015) and others). The hardness of sapphire of about 21 GPa is almost independent of the crystallographic orientation of the surface being indented (Sinani et al. 2009). This value of the hardness agrees very well with the data in Fig. 4.1a that were measured with the original version of Fischerscope H100 using the simple method of Doerner and Nix.

The incorrect, too high value of the hardness of sapphire of 28–30 GPa obtained by the Oliver and Pharr method when the instrument is calibrated for a constant stiffness of fused silica, in contrast to the results of Fig. 4.1a, has been reported in several publications and books without any critical analysis (e.g., Fischer-Cripps 2004, Appendix 5; Dub et al. 2014). It is probably related to the fact that sapphire has different elastic–plastic behavior and higher Young's modulus as compared to its hardness than fused silica. No systematic study of this issue has been conducted so far, although some improvements, such as "variable intercept factor," have been discussed (Chudoba and Jennett 2008). The complex elastic–plastic transformation and pop-in phenomena that occur in sapphire upon indentation at small load of few mN and displacement < 100 nm will not be discussed here (see, e.g., Dub et al. 2014). With reference to Fig. 4.1a, we emphasize that these phenomena do

not occur at larger load where the correct, load-invariant hardness of about 21 GPa is found.

We shall not continue the discussion of the methods which should be used for the measurement with the automated load-depth sensing "nanoindentation" technique. We only emphasize that the example of sapphire should be a warning that much care should be taken when measuring hardness of super- and ultrahard materials using the "nanoindentation" technique. The so-called tip area correction is obviously a calibration of the instrument using a material with given elastic–plastic mechanical properties, and this calibration does not need to apply to a material with different elastic–plastic behavior.

In order to illustrate the problems which may happen when using the "nanoindentation" technique without a deeper analysis of the method, we show in Fig. 4.2 the mistakes which happen when the so-called corrected (in fact "transformed" by the polynomial fit according to Doerner and Nix as explained above) indentation curves are incorrectly taken as the true load–depth dependencies, as done in Fischer-Cripps et al. (2012). Figure 4.2a is Fig. 2 from Veprek et al. (2003c). One can see that the hardness of the nanocomposite coatings of 49.7 GPa obtained from the early version of Fischerscope H100 which used the Doerner and Nix method for calibration (Doerner and Nix 1986), that of 48.4 GPa obtained from the size of the remnant indent measured by scanning electron microscope, SEM, and those obtained by linear extrapolation of 20, 30, and 35 % of the initial part of the unloading curve, agrees with the average value of the 48.7 GPa within 1.6 %. In contrast, the value obtained by fitting this curve using the Oliver and Pharr method yields only 28.8 GPa, lower by a factor of 1.7. However, when the method of Oliver and Pharr is applied to the "as measured" curve, which is the actual load-depth dependence, hardness value of 52.3 GPa is obtained. This value is slightly higher than the correct one because of neglect of the tip rounding. This difference is relatively small because the indentation depth of about 0.6 μm was sufficiently large so that the neglect of the tip rounding causes only a relatively small error.

In order to emphasize this point, we show in Fig. 4.2b the hardness of a reference industrial diamond in dependence on the applied load. The results obtained from the early version of Fischerscope H100 are displayed as asterisks. When applying the Oliver and Pharr method to the "as measured" indentation curves and approximately accounting for the tip rounding, hardness of about 110 GPa is obtained. This is in a reasonable agreement with the values of about 104 GPa obtained by the early version of Fischerscope H100, which used the method of Doerner and Nix,[3] and with the value of 110 GPa measured on the same diamond by Fischer-Cripps et al. (2006) who used the method of Oliver and Pharr. However, when the method of Oliver and Pharr is applied to the "corrected" (i.e., transformed by the polynomial function) curve of the Fischerscope H100, an incorrect hardness of about

[3] One has to consider the fact that the values obtained from the individual measurements show relatively large scattering of up to 10 %.

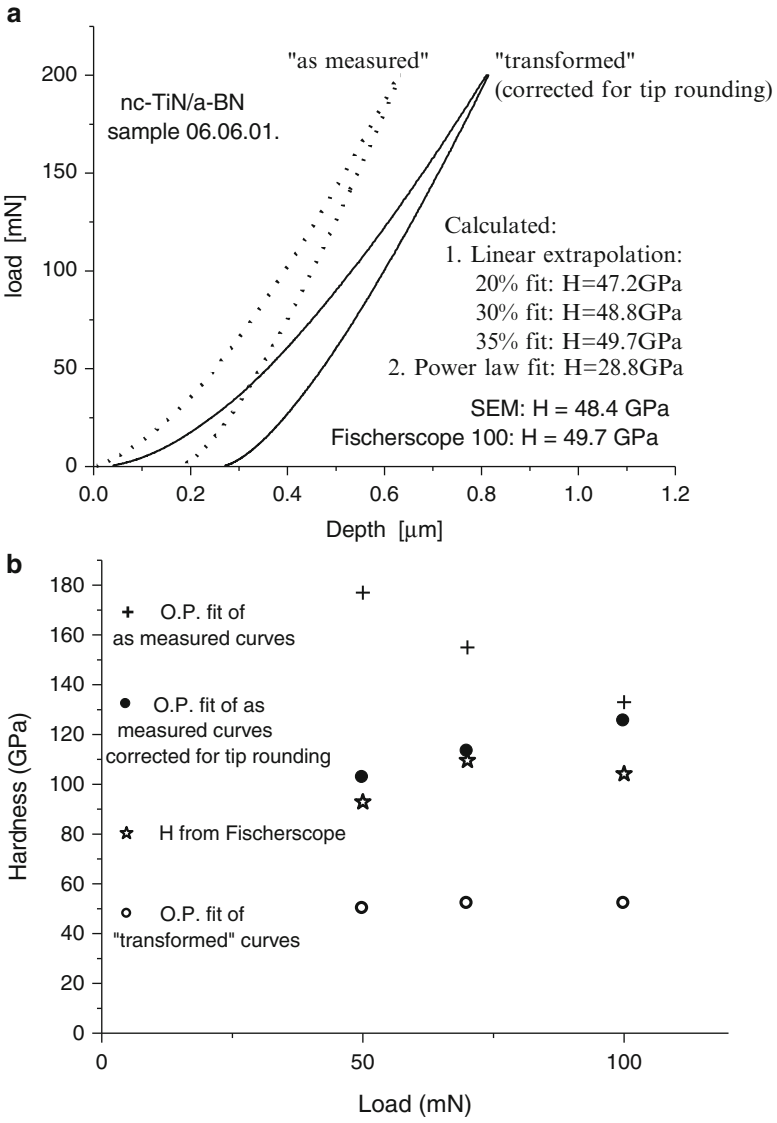

Fig. 4.2 (**a**) "As measured" and "calibrated" indentation curves into superhard nc-TiN/a-BN coatings. The apparent "hardness" obtained from the calibrated and as measured curve using Oliver and Pharr method (Oliver and Pharr 1992) is 28.8 and 52.3 GPa, respectively (reproduced from Fig. 2 in Veprek et al. 2003c with permission). (**b**) *Crosses*, hardness of diamond vs. maximum applied load calculated by means of Oliver and Pharr method from the "as measured" indentations curves without tip area corrections; *full circles*, after a simple tip correction assuming a tip radius of about 0.7 μm, roughly in agreement with the tip rounding reported earlier (Veprek-Heijman et al. 2009); *stars*, hardness obtained from Fischerscope H100; *open circles*, incorrect values of "hardness" obtained from the fit—using the Oliver and Pharr method—of the indentation curves which have been calibrated according to Doerner and Nix method (Doerner and Nix 1986)

50 GPa, lower by about a factor of two, is obtained. This has been shown by the authors already in 2003 (see Fig. 3 in Veprek 2003c). Exactly this mistake happened to Fischer-Cripps et al. in their paper where they claim that we measured the hardness of the ultrahard nanocomposite coatings incorrectly, "too high by a factor of two" (Fischer-Cripps et al. 2012).

Another effect, which may falsify the hardness measurement when using the automated load-depth sensing technique, is the pileup that often occurs during indentation into ductile materials. During the indentation, the ductile material flows up along the diamond indenter, thus decreasing the apparent indentation depth that is measured by the automated load-depth sensing techniques. As a result, the indentometer is sensing smaller indentation depth than the correct one, thus giving an incorrect, higher hardness. The only way to avoid this error is to measure the size of the remnant indentation by a microscope. Many modern "nanoindentometers" are equipped with atomic force microscope and thus enable this task. Because pileup is relatively unlikely to occur when indenting superhard materials, we don't discuss this issue here in any more detail and refer to the literature instead (Taljat et al. 1998; Bolshakov et al. 1997; Bolshakov and Pharr 1998).

From this short overview of possible artifacts that may occur when using the "nanoindentation," it should be clear that the ultimate test remains the classical two-step indentation method, where the size of the remnant plastic indent is measured by a microscope after unloading. This statement is further supported by the fact that many super- and ultrahard materials display ISE that is not related to the finite radius of the indenter tip (see next section) which makes it necessary to use large load of several N that many of the modern sophisticated "nanoindentometers" do not provide. We refer to the paper by Brazhkin et al. who emphasized these facts already in previous studies (Brazhkin et al. 2004).

2.3 *Indentation Size Effect and the Possible Errors of the Hardness Measurements*

As already mentioned, the indentation size effect (ISE) can have a variety of origins, including the rounding of the indenter tip. This can be compensated for by a careful calibration of the instrument ("tip area correction").

Another possible reason for the appearance of ISE is the incomplete development of the plastic deformation beneath the indenter at low applied load which leads to an apparently higher strength and hardness of materials when tested at nanoscale. When materials, such as aluminum or copper, are tested by "nanoindentation" with a load of a few 10 μN where the indentation depth amounts to only a few 10 nm, the plasticity cannot fully develop and the behavior of such materials corresponds to that of an ideal perfect single crystal (see, e.g., Gouldstone et al. 2001; Li et al. 2002; Van Vliet and Suresh 2002). Such a

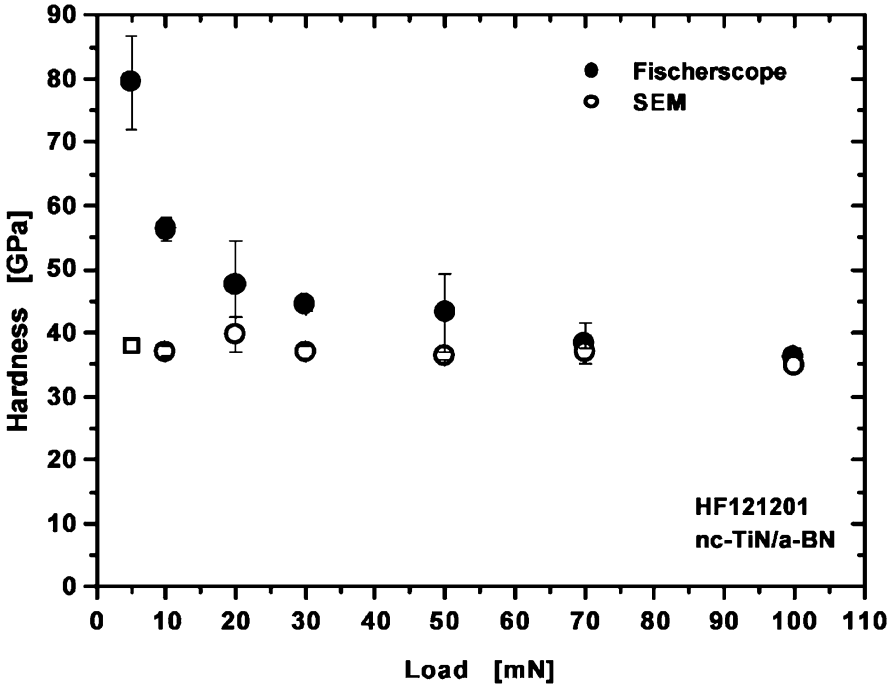

Fig. 4.3 Hardness of a 6 μm thick nc-TiN/BN nanocomposite coating vs. applied load obtained from indentometer Fischerscope H100 after tip area correction (*full symbols*) and from the area of remnant plastic deformation determined by calibrated scanning electron microscope (from Veprek et al. 2003a) with permission)

behavior resembles the strengthening of nano-sized materials (Zhu et al. 2008) although it is also found in large-grain polycrystals when indented at nanoscale. We refer to a recent review by Pharr et al. for further details regarding ISE (Pharr et al. 2010). Here we only emphasize that the hardness measurement by indentation has to be done at sufficiently high load to assure that the material operates in a regime of fully developed plasticity for which the criterion is that the hardness is load invariant as described by Meyer already some time ago (Meyer 1908).

Even if a sufficiently high load is used and the tip area correction carefully done, ISE may occur due to other artifacts. In Fig. 4.3 we show such an example: The hardness obtained from the area of the remnant plastic deformation by calibrated scanning electron microscope (SEM) is constant for all loads between 5 mN and 100 mN used, but the hardness values obtained from the indentometer show a pronounced ISE, approaching the correct value only at a load of 70 mN. As described in our earlier paper to which we refer for further details, this ISE was due to anelastic[4] deformation of the steel substrate (Veprek et al. 2003a).

[4] Anelasticity is a reversible, time delayed deformation described, e.g., in Gottstein (2004).

ISE which cannot be corrected for by the "tip area correction" routine has its origin in the mechanical properties of the material being tested. Figure 4.4a shows an example of strongly pronounced ISE in moissanite (6H-SiC—one of many modifications of silicon carbide) where a load of about 100 N is needed to reach the regime of load-invariant hardness (Brazhkin et al. 2004). Because these authors refer to an unpublished work, we cannot discuss the possible reason for such large ISE. Possibly, it can lay in the easy formation of stacking faults between the SiC double layers which are well known to occur in SiC. This easy formation of the stacking faults has, as a consequence, also the large number (more than 200) of different polymorphs of this material. Possibly, many of such polymorphs appear during the indentation into this material.

Another example of ISE is shown in Fig. 4.4b for ReB_2 which has "low compressibility" (large elastic moduli) and, therefore, has been suggested to be superhard (Chung et al. 2007). However, as seen in Fig. 4.4b by extrapolation of the measured data to larger load, the load-invariant hardness of ReB_2, which would be obtained at a larger loads than those used in this measurement, is less than 30 GPa. Obviously, ReB_2 is not superhard as incorrectly claimed in that paper (Chung et al. 2007) and in several follow-up papers which refer to the value of 48 GPa measured at the low load of 0.46 N. The reasons for the slow approach of the apparent hardness toward the correct load-invariant value are most probably electronic instabilities and concomitant structural transformations to other unstable and metastable structures with lower shear resistance than the original equilibrium structure that occur under a finite shear strain, as shown by Zhang et al. (2010). We refer to the paper of Zhang et al. and to the recent review (Veprek 2013) for further discussion of this problem.

Because electronic instabilities upon a final shear are likely to occur in materials with complex atomic valence orbitals, such as d-metals where electronic instabilities upon shear due to crystal field splitting are likely to occur (Zhang et al. 2010, 2014; Veprek 2013), measurement of the hardness as function of applied load has to be done to verify if the measured values are indeed load invariant. The data presented in Fig. 4.3 clearly show that the ISE is absent in the nanocomposites at loads of ≥ 5 mN because the 3 nm small TiN nanocrystals approach the ideal strength and therefore deform only elastically, whereas the interfaces are the carrier of the plastic flow (see below).

Also diamond transforms to graphite upon shear of > 0.3 in the (111)[11–2] slip system as shown by first-principles studies (e.g., Veprek et al. 2010a) and experimentally observed by Raman scattering of the indented area (Gogotsi et al. 1999). However, because of the relatively simple electronic structure of diamond, this transformation requires a very high shear stress. Therefore, diamond is ultrahard. Its correct, load-invariant hardness can be obtained already at relatively low load of ≤ 30 mN [see, e.g., Fig. 12a in Veprek et al. (2005)]. However, nanotwinned diamond with average distance between the twins of about 4 nm displays a pronounced ISE reaching the load-invariant hardness of about 200 GPa only

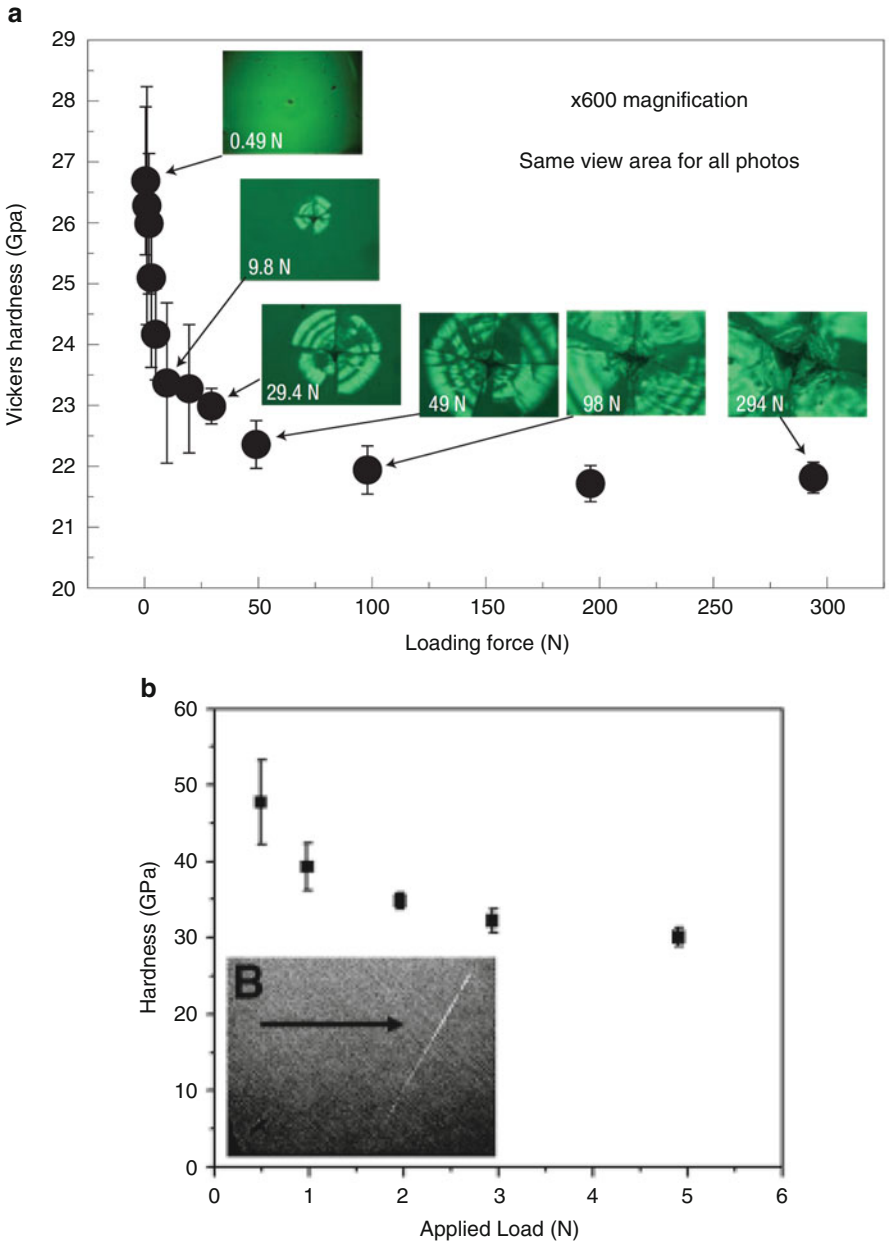

Fig. 4.4 (**a**) Vickers hardness of moissanite (6H-SiC) vs. the applied load together with the micrographs of the indents (from Brazhkin et al. 2004, with permission). (**b**) Hardness of ReB_2 vs. the applied load (from Chung et al. 2007, with permission)

at a load of 5 N [see Fig. 3a in Huang et al. (2014) and Fig. 4 in Xu and Tian (2015)].[5]

As already mentioned, there is no any unambiguous rule which could predict at what load the load-invariant value of hardness can be achieved in a given material. As a somewhat vague rule of thumb, we would suggest that only materials with simple electronic structure, such as diamond, or those where the regions of the plastic flow are well defined, such as the grain boundaries in the superhard nc-TiN/Si_3N_4 and related nanocomposites (Veprek et al. 2010a; Veprek 2013; Ivashchenko et al. 2015), the ISE is likely to be small, and the load-invariant hardness can be measured at relatively low load of few mN. For example, in the nc-TiN/Si_3N_4 nanocomposites with a thickness of 5–13 μm, the load-invariant superhardness has been achieved already at a small load of ≥ 5 mN [see Figs. 3 and 28a in Veprek (2013)]. In materials with a complex electronic structure, such as the borides of d-metals, a large load of up to several N is needed. This may be a limitation for the use of the modern instruments for "nanoindentation" to determine hardness of super- and ultrahard materials, because many of these instruments do not provide a sufficiently large load.

2.4 *Measurement on Hard and Superhard Coating on Softer Substrates*

Hard and superhard coatings are industrially used as wear protection coatings on tools for machining (drilling, milling, turning, etc.), injection molding, stamping, and the like (see, e.g., Inspektor and Salvador 2014; Mayrhofer et al. 2006; Veprek and Veprek-Heijman 2008). Cemented carbide (WC-Co) and high-speed steel (HSS) are used as materials of the tools. Hard coatings are used also in machine parts; in medicine, as decorative coatings; and in many other applications. In almost all these cases, the substrate is softer than the coating. Thus, the question arises as to what conditions must be met to make sure that the hardness is measured correctly in such a case. This problem has been discussed in some detail in the recent paper (Veprek-Heijman and Veprek 2015) and references quoted therein. Here, we shall give a short summary of this problem.

As we have seen in the previous section, the indentation load and concomitant indentation depth must be sufficiently high to assure that the material being

[5] One might doubt if it is possible to measure hardness of 200 GPa using diamond indenter because the diamond indenter has a hardness of only 80–100 GPa. This is possible because the diamond indenter is loaded mainly in compression, whereas the material being indented is loaded predominantly in shear (see, e.g., Fig. 13.8 in McClintock and Argon (1966), p. 454 and also Fig. 29 in Veprek (2013) that shows the flow of the material in the indenter due to the indentation into an ultrahard material). Diamond as well as the majority of intrinsically strong materials sustains up to eight times higher stress in compression than in shear. The recent estimate of the maximum pressure that diamond can sustain suggests a lower limit of about 420 GPa (Eremets et al. 2005).

measured operates in the regime of fully developed plasticity where the correct, load-invariant hardness is obtained. The corresponding "minimum indentation depth" may be as small as 100 nm for simple nitrides, carbides, or nanocomposites, but several μm may be needed for some materials that display a slow approach to the load-invariant value. The high elastic strain in the hard coatings may cause plastic deformation of the softer substrate even when the plastically deformed zone in the coatings beneath the indenter is relatively small and does not reach the interface to the substrate. In that case, the measured "compound hardness" of the coatings and softer substrates is obtained. When the hardness is measured, at sufficiently thick coatings, as function of the increasing applied load (or indentation depth), the obtained values change from that of the coatings to the compound hardness of the system coatings/substrate that continuously decreases toward the hardness of the substrate. Several models have been proposed to evaluate the correct hardness of the coatings from the compound measured hardness of the system coatings/substrate (e.g., Johnsson and Hogmark 1984; Korsunsky et al. 1998; Bull et al. 2004). However, the range of the load where these models work sufficiently well is relatively narrow, and high-quality experimental data are needed. Therefore, these models are of limited use and shall not be discussed here.

The linear FEM work of Sun et al. (1995a, b) showed the influence of the ratio of the yield strength of coatings and substrate and of the tip radius of a rigid indenter on the loading curve in the indentation experiment. However, these calculations were limited to linear FEM and to thin coatings of limited hardness. Here, we shall summarize the results of nonlinear finite element modeling (FEM) which has been recently conducted to determine the thickness of the coating of a given hardness on typical substrates used, such as steel, silicon wafer, and cemented carbide (Veprek-Heijman and Veprek 2015). He and Veprek (2003) conducted similar studies using the linear FEM, but limited in the study as regards the range of hardness of the coatings and the type of the substrates. Therefore, we shall not discuss them here.

The nonlinear FEM accounts for the pressure enhancement of elastic moduli[6] and concomitant increase of plastic flow resistance due to the pressure beneath the indenter that develops during the hardness measurement (Veprek et al. 2007). As shown in Veprek et al. (2007), the distribution of the volumetric strain (elastic deformation, Fig. 11 therein) and deviatoric strain (plastic deformation, Fig. 12) under the indenter differ significantly for the linear and nonlinear FEM. This emphasizes the need for using the nonlinear constitutive material model to calculate how the strains in the coatings are transferred into the substrate and when they may cause its plastic deformation.

[6] Under isostatic pressure the elastic moduli are enhanced. For example, the bulk modulus at pressure p is given by $B(p) = B_0 + b \cdot p$ where B_0 is the bulk modulus at zero pressure and b is the proportionality factor which is typically between 3 and 5 for the majority of materials (Rose et al. 1984).

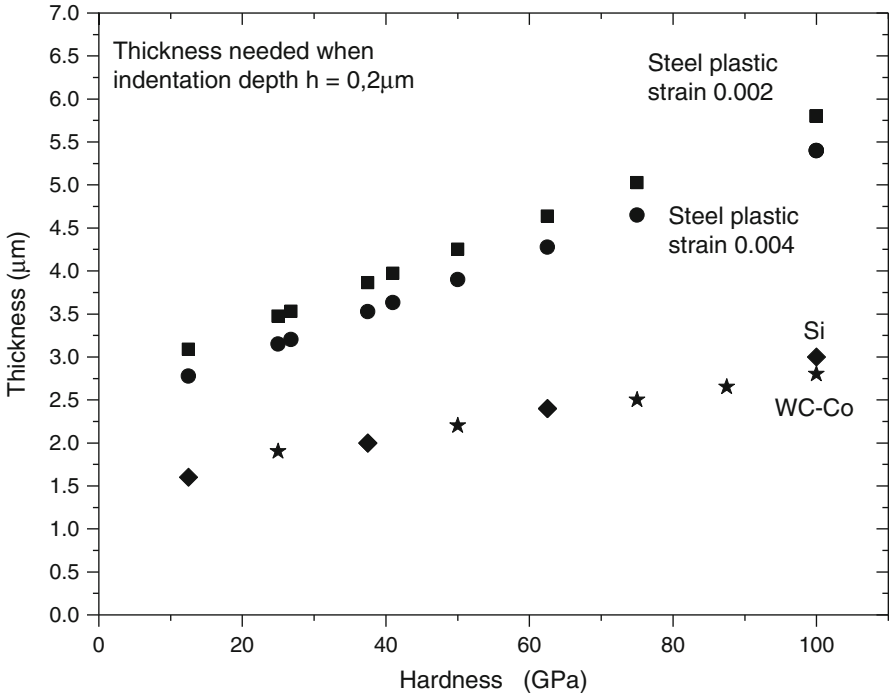

Fig. 4.5 Minimum thickness of the coatings of the given hardness that is needed for the correct measurement of the hardness of the coatings (see text). For steel substrate we show data for plastic strain of 0.002 and 0.004 to illustrate that this difference has only small effect on the t/h ratio. *Full squares*, steel substrate with plastic strain 0.002; *full circles*, steel substrate with plastic strain 0.004; *full diamonds*, substrate Si; *asterisks*, substrate WC-Co cemented carbide

In our nonlinear FEM, we calculated the thickness of the coatings of a given hardness that is needed to avoid plastic deformation of the given substrate when the minimum indentation depth is 0.2 μm, using a dull indenter as explained above (Veprek-Heijman and Veprek 2015). Figure 4.5 shows the minimum thickness of the coatings of different hardness on three different substrates, as indicated, that is needed to avoid plastic deformation of the substrate (i.e., plastic strain ≤ 0.002 or 0.2 %). For steel substrate we show also the results for somewhat larger onset of the plastic strain of 0.004 to illustrate that in this range of the strain, the difference is relatively small (Veprek-Heijman and Veprek 2015).

Usually, one refers to the "Bückle's rule" according to which the indentation depth should not exceed 10 % of the thickness of the coatings in order to avoid the plastic deformation of the softer substrate (Bückle 1965, 1973). In our recent paper (Veprek-Heijman and Veprek 2015), we presented the dependence of the ratio of thickness of the coatings to the indentation depth which is needed to avoid plastic deformation of the substrate. Obviously, this rule does not apply for coatings with hardness ≥ 10 GPa on steel and for coatings with hardness of ≥ 30 GPa on Si wafers and cemented carbide. Clearly, Bückle's rule does not apply when measuring the hardness of superhard materials.

Thus, the reader should use Fig. 4.5 of this paper as rough guideline to estimate which thickness of coatings with given hardness on a given substrate is needed for correct measurements. However, the reader has to consider that these data apply for indentation depth of only 0.2 μm. If large indentation depth is needed to achieve the load-invariant regime of the measured hardness, correspondingly thicker coatings are needed. This has been emphasized and followed in our papers on the superhard nanocomposites from the very beginning (Veprek and Reiprich 1995), but ignored in many papers of other researchers where "superhardness" of 40–60 GPa has been reported on 1–2 μm thick or even thinner coatings deposited on steel or Si substrates. For example, Zhang et al. reported "hardness" of up to 38 GPa for 0.16–0.41 μm thick Ti-Si-N coatings which is obviously incorrect (Zhang et al. 2004). Unfortunately, there are many other examples of reports on "superhard" coatings where the hardness has been incorrectly measured [see some examples quoted in Veprek-Heijman and Veprek (2015)].

When the hardness of ultrahard coatings is measured, the required thickness may be too large for unambiguous verification that the obtained hardness is really load invariant. For example, in the case of ultrahard coatings on steel or silicon, the required thickness would be several tens of micrometers. Such coatings are difficult or impossible to prepare because of biaxial compressive stress present in coatings deposited by plasma chemical or physical vapor deposition. In such case, one has to measure the compound hardness of the system coatings/substrate up to sufficiently large load of at least 500 mN. Afterward, one has to use the nonlinear FEM to verify the data obtained at large loads, where the plastic deformation of the softer substrate occurs or even dominates. Only when the measured curve can be reproduced using the nonlinear FEM with one constant value of the hardness of the coatings can the value of hardness be considered correct.

This is illustrated in Fig. 4.6 which shows the comparison between the measured hardness of 7.3 μm thick ultrahard quasi-ternary nc-TiN/Si_3N_4/$TiSi_2$ coatings on steel (with an additional interlayer of 3.4 μm TiN), determined from the scanning electron micrographs and calculated by the nonlinear FEM. With reference to Fig. 4.3, we note that the indentation size effect occurs at low load of less than 5 mN for the nc-TiN/BN coatings. In Fig. 28a of Veprek (2013), we have an example of 13.8 μm thick nc-TiN/Si_3N_4 coatings which show load-invariant hardness from the smallest load of 20 mN used, i.e., the indentation size effect occurs at smaller load. There are more examples which show that in the nanocomposites under discussion here, the ISE is limited to much smaller load because the plastic flow occurs in the grain boundaries (Ivashchenko et al. 2015). Therefore, also in the example shown in Fig. 4.6b, the indentation size effect is not seen because the lowest load used was 50 mN.

In the FEM calculations, the only adjustable parameter has been the yield strength of the coatings as described in Veprek-Heijman et al. (2009).[7] One can

[7] The reader should note that other parameters, such as elastic moduli of the materials of coatings and substrate as well as their dependence on pressure, the yield strengths, and hardness of the substrate, enter the FEM calculations as constant materials parameters.

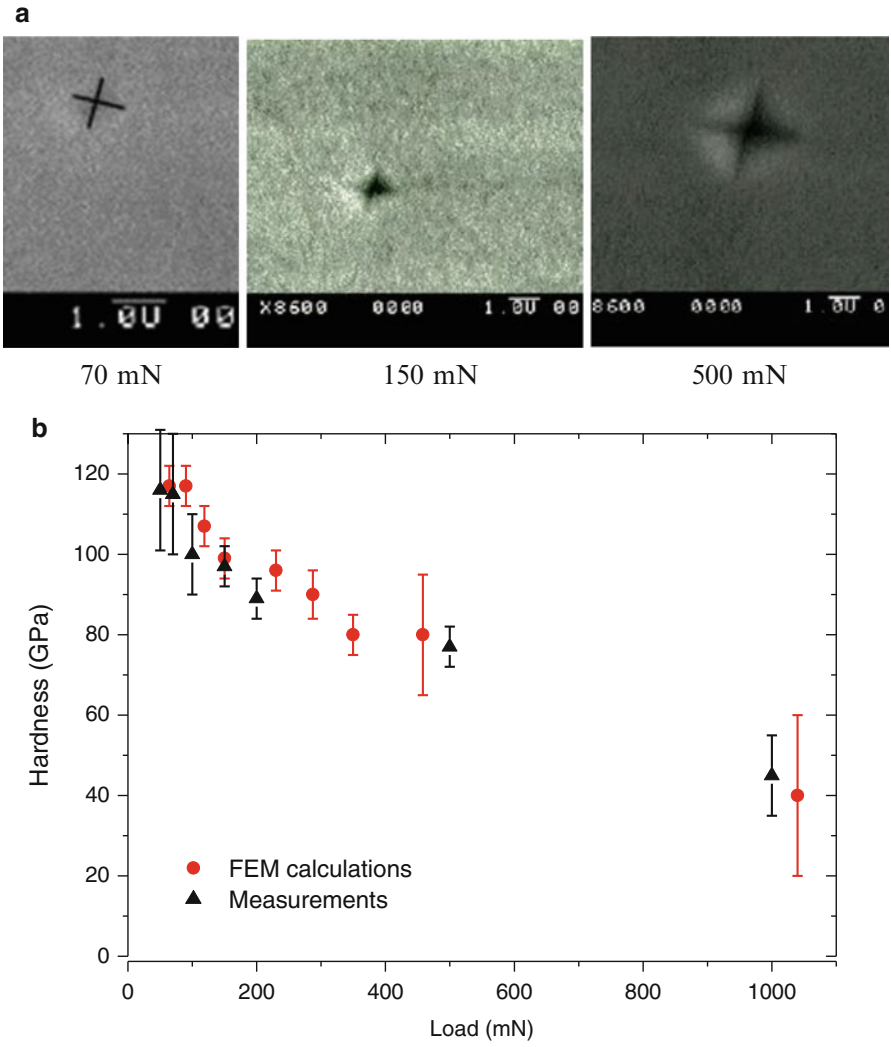

Fig. 4.6 (**a**) Examples of scanning electron micrographs of remnant indentations into the ultrahard nc-TiN/Si_3N_4/$TiSi_2$ nanocomposites at a given load as indicated, (**b**) hardness vs. maximum applied load: *crosses* are the experimental data from (Veprek and Veprek-Heijman 2012), and *open symbols* are the values calculated by the present nonlinear FEM (Veprek-Heijman and Veprek 2015)

see that the experimental data agree very well with the nonlinear FEM calculations up to high load of 1000 mN. Thus, the hardness of about 115 GPa measured at load of 50 and 70 mN is the correct hardness of the coatings because the nonlinear FEM reproduces very well the compound hardness of the system coatings/substrate up to the highest load of 1000 mN. We emphasize again that indentation size effect can be ruled out in these data. Note that at a load of 500 mN, the compound hardness is

still close to 80 GPa. As discussed in Chap. 6, in these nanocomposites the grain boundaries are the carrier of the plastic flow, whereas the 3–4 nm size TiN nanocrystals deform only elastically. For this reason the load-invariant hardness is measured already at the low load of 50–70 mN.

In conclusion to this subsection, we emphasize that the hardness of hard and superhard coatings can be correctly measured only when the coatings are sufficiently thick to avoid the plastic deformation of the substrate and to verify that the measured value of hardness is load invariant. In the case of ultrahard coatings, where the required thickness of the coatings would be too large, nonlinear FEM has to be used to verify if the compound hardness of the system coating/substrate yields a correct value of the hardness of the coating. Application of the Bückle's rule, according to which the indentation depth should not exceed 10 % of the thickness of the coatings, is not justified for superhard coatings on soft substrates.

3 Measurement of Elastic Moduli

The Young's modulus is conventionally determined in a classical tensile stress test. However, the preparation of the sample for such test is difficult or impossible when the measurement should be done with hard and superhard materials. Moreover, novel ultraincompressible materials, which are believed to be possibly superhard, are often prepared in very small quantities and as small grains which are not suitable for the classical measurements. Therefore, other methods for the determination of Young's and other moduli have to be used.

In principle, Young's modulus might be evaluated by the load–depth-sensing technique using the method of Oliver and Pharr that enables to determine the "reduced modulus," E_r, given by Eq. 4.2 (1992). Here, E is the Young's modulus and ν is the Poisson's ratio of the coatings and E_i and ν_i are the same parameters for the indenter (Oliver and Pharr 1992):

$$E_r = \frac{1-\nu^2}{E} + \frac{1-\nu_i}{E_i} \tag{4.7}$$

Although this method works reasonably well for softer materials, its application to superhard materials is not guaranteed because the analysis of the unloading part of the indentation curve is based on linear elastic–plastic behavior. This alone may cause errors of the evaluated Young's modulus at more than 20 % (Veprek RG et al. 2007). Moreover, the concept of the reduced modulus and applicability of the Sneddon's solution on which the concept of the measurement is based have been questioned by several researchers (e.g., Bolshakov and Pharr 1997; Hay et al. 1999; Chaudhri 2001; Chaudhri and Lim 2007; Rodriguez et al. 2011). We don't want to discuss this complex issue here. Instead we shall discuss other techniques which are suitable for the determination of elastic moduli of superhard materials. Because, as mentioned, the classical tensile stress–strain test, from which Young's modulus can

be determined, is difficult to conduct with superhard materials and coatings, we shall focus on other methods of the measurements which do not suffer from this difficulty.

The bulk modulus B can be determined from high-pressure X-ray diffraction (XRD), when small samples of the material are inserted into diamond anvil cell and exposed to high pressure and the change of the spacing of the crystallographic plains as function of applied pressure is determined from XRD. This method is described in a number of papers to which we refer for further details (e.g., Jayaraman 1983; Cynn et al. 2002). It has been also used to measure the bulk modulus of superhard nanocomposites (Veprek et al. 2010b). The sample preparation is simple because small quantity of powder of a grain size of > 10 μm is sufficient for such measurements. The only problem may be that synchrotron radiation is needed for such studies, but this should not be a serious problem nowadays. In such experiments, also the pressure dependence of the bulk modulus is obtained (e.g., Veprek et al. 2010b).

Young's modulus E of thin films can be measured by the vibrating reed method. In this case, the coatings are deposited on both sides of an elongated substrate strip made of an elastic metal that is subsequently fixed on one end, and its mechanical oscillations are excited by means of an appropriate actuator. The resonant frequency of the oscillating reed is measured, and the Young's modulus of the coating is calculated from a well-established formula (Li et al. 2004). This method can be simultaneously used to evaluate the internal friction of poly- or nanocrystalline coatings which provides an important information about the structural stability of the grain boundaries, segregation of the phases, and formation of stable poly- or nanocrystalline structure (see Li et al. 2004, 2005).

Probably the most convenient method for measuring elastic moduli is Brillouin surface scattering (BSS; see, e.g., Zinin et al. 1999; Abadias et al. 2014a, b) which allows to simultaneously determine the Young's modulus, E, and shear modulus, G, which also yield the Poisson's ratio ν due to the relationship $G = E/2(1 + \nu)$ (see, e.g., Kelly and Macmillan 1986). In such a way, all three moduli can be compared using the well-known relationships between them (Kelly and Macmillan 1986). Using the combination of high-pressure XRD, vibrating reed, and Brillouin surface scattering, all three moduli of the nc-TiN/Si_3N_4 nanocomposites have been determined with high accuracy and agreement between all three methods within less than 5 % as shown in Table 4.1 (Veprek et al. 2003c). Obviously, the vibrating reed, surface Brillouin scattering, and high-pressure XRD are the methods of choice for the measurements of the elastic moduli of superhard and ultrahard materials.

Table 4.1 Average values of Young's E, bulk B, and shear modulus G measured on TiN and on superhard nc-TiN/Si_3N_4 nanocomposites by vibrating reed, high-pressure XRD, and surface Brillouin scattering using a large number of samples (see Veprek et al. 2003c)

E (GPa)	B (GPa)	G (GPa)
445 ± 20	295 ± 15	195 ± 15

Ultrasonic interferometry can be used for the determination of second-order elastic constant of bulk samples from which elastic moduli B and G can be calculated using the well-known formulae (see review by Jacobsen et al. 2005). Thus, also the Poisson's ratio and Young's modulus can be obtained. The recent development of this technique into the gigahertz range allowed one to measure elastic moduli with high precision of about 0.1 and 1 % for samples of 1 and 0.1 mm size, respectively (Chang et al. 2014). The measurements can also be done on samples placed in diamond culets and exposed to high pressure. As far as we know, this method has not been used so far for measurement of elastic properties of thin films on a substrate. Most probably, the usually small thickness of the coatings and the presence of the substrate will make it difficult.

4 Measurement of Stress in the Films Deposited on a Substrate

Because optimally processed superhard bulk materials should be free of noticeable stresses, we shall concentrate on the measurement of stress in polycrystalline thin films on a substrate. One has to distinguish between the random stress which originates from the grain boundaries and biaxial stress of the coatings that may have a variety of origins. However, we have to keep in mind that random strain and concomitant stress are likely to appear in the recently prepared nanocrystalline diamond (Chang et al. 2014) and in nano-twinned c-BN (Tian et al. 2013) and diamond (Huang et al. 2014; Xu and Tian 2015). No such studies have been done so far.

The random stress has its origin in dislocations or in strain within the grain boundaries of polycrystalline material that causes random dilatation and compression of the crystallites, which contributes to broadening of the Bragg reflection in XRD. The most reliable determination of the random strain provides the integral method of Warren and Averbach, which uses the Fourier transform to distinguish between the broadening of the Bragg reflections due to the random strain and broadening due to finite crystallite size (Warren and Averbach 1952; Klug and Alexander 1974; Mittemeijer and Welzel 2008). The frequently used method of Williamson and Hall (Williamson and Hall 1953; Hall 1949; Hall and Williamson 1951; Pelleg et al. 2005) assumes additive contribution of the broadening due to finite crystallite size and random strain to the experimentally measured peak width that is however valid only if the peaks have Cauchy profiles (Klug and Alexander 1974, p. 635). This is generally not the case. Therefore, the integral method of Warren and Averbach has to be used. The random strain and concomitant stress within the grain boundaries in the superhard nc-TiN/Si_3N_4 nanocomposites with 3–4 nm size TiN nanocrystals can reach high values of ≥ 7 GPa [see Fig. 5 in

Niederhofer et al. (1999)] which may—in long terms—destabilize some metastable phases within the grain boundaries [see Veprek (2013) and references therein].

Biaxial stress in thin films may be due to mismatch of the coefficient of thermal expansion, or to ion bombardment during the film growth, or to a variety of other effects. The stress may also change with the depth in the film and in particular during the film growth. Because the discussion of the different type of the stress is beyond the scope of this chapter, we limit our discussion only to the compressive biaxial stress that is caused in the films by energetic ion bombardment during growth in plasma chemical and physical vapor deposition and is important for, e.g., the adherence of coatings on tools.

A medium compressive stress of 1–3 GPa, which is obtained by bombardment of the growing film with low-energy ions [see, e.g., Fig. 1 in Veprek et al. (1987)], is beneficial because it makes the film dense which avoids incorporation of impurities when the film is—after the deposition—exposed to air. However, a too large compressive stress causes undesirable delamination. For these reasons the measurement of the stress is needed. This can be done by measurement of the shifts of the Bragg peaks in XRD using the so-called $\sin^2\varphi$ method (Noyan and Cohen 1987). However, there are several assumptions behind this method which are not always met in the praxis. Therefore, the simple method of the measurement of the curvature of the film/substrate system after the deposition of the film is, according to the experience of the present authors, much easier and reliable. The measurement can be done after the deposition, but the evolution of the stress during the growth, which may be quite complicated, can be also done in situ during the film growth (see, e.g., Fillon et al. 2010; Chason 2012; Abadias et al. 2008, 2011, 2013, 2014c). The stress in the film is evaluated from the bending of the system film/substrate using the Stoney's formula (Stoney 1909; Janssen et al. 2009). The multiple laser beam reflection from the surface of the film (or from the substrate) is a more elaborate technique to measure the bending of the system substrate/film (Chason 2012), but for the "daily" deposition experiments, the determination of the stress from the bending measured by optical microscope is in most cases sufficient.

Stress in the coatings may also influence the measurement of the mechanical properties of the thin films, in particular by "nanoindentation." We refer to the published papers for further details (e.g., Bolshakov et al. 1996; Tsui et al. 1996; Keutenedjian Mady et al. 2012). The hardness of transition metal nitrides deposited by reactive sputtering under ion bombardment at relatively low temperature can reach very high values [e.g., up to almost 80 GPa for TiN (Musil et al. 1988) and more than 40 GPa for a variety of nanocomposites consisting of hard transition metal nitride and ductile metal that does not form nitride (Musil 2000)], but upon annealing to ≥ 500 °C, the hardness decreases to its usual value (Karvankova et al. 2001). These coatings are discussed in Chap. 6.

5 Tensile Yield Strength

Tensile yield strength is the applied tensile stress where—after unloading—the remnant plastic deformation amounts to 0.2 %, i.e., plastic strain 0.002 (Gottstein 2004, p. 203). It can be exactly measured only in a tensile test, which—as already discussed—is not an easy task to conduct with superhard materials. Moreover, special sample preparation is required for the tensile test, which is very difficult to do when the material is available only as small species. Eremets et al. (2005) determined the yield strength of diamond of about 130–140 GPa by measuring the pressure distribution over the diamond anvils and by using the theory of elasticity. This method can be applied to other superhard materials.

As a very rough estimate, one may use the relation between the hardness H and tensile yield strength Y, $H = C \cdot Y$ with the constraint factor $C \approx 2.6$–2.8 that has been calculated by several researchers and more recently also by means of nonlinear FEM (Veprek-Heijman et al. 2009). A detailed discussion of the meaning of the constraint factor can be found in Veprek (2013), Appendix B.[8] When the hardness is measured correctly, the uncertainty of the yield stress should not be more than about 20 %. But, as mentioned, the reliability of such values is limited.

6 Summary

A correct measurement of hardness of super- and ultrahard materials must assure that the reported value is load invariant. In many cases of intrinsically super- and ultrahard materials, this can be achieved only at very large load of several N. Because the majority of the modern automatic load–depth-sensing instruments ("nanoindenters") do not allow one to apply high loads of several N, and because of many other possible artifacts that may occur when using this technique, the most reliable way to measure the hardness is the classical two-step method, where after unloading, the size of the remnant plastic indentation is measured with a microscope. In this case one also avoids the problem arising from different elastic–plastic behavior of different materials used for the calibration of the "nanoindentometer" and materials being measured. We have shown several examples of possible artifacts which can occur when the "nanoindentometers" are used.

[8] It has been claimed that for extrinsically superhard materials, the expanding cavity model (Hill 1950) should be used that yields a much smaller value of the constraint factor (Fischer-Cripps et al. 2012). However, in the expanding cavity model, only radial flow of material occurs, whereas in the superhard nanocomposites, the flow resembles that of the slip-line fields (Hill 1950; McClintock and Argon 1966) that yields the constraint factor of 2.7–3 [see Veprek (2013), Appendix B, and Fig. 29 therein]. The expanding cavity model is useful for elastomers, some polymers, and materials that plastically deform by densification, such as silicate glasses, but not for superhard ceramic materials.

When measuring on super- and ultrahard materials, an initially sharp diamond indenter undergoes plastic deformation which finishes at a "radius" of about 0.5–0.7 μm. Therefore, the hardness measurement on super- and ultrahard materials can be done only with a dull indenter. This requires relatively high applied load to develop full plasticity in the material being tested.

A particular problem is the measurement on super- and ultrahard coatings deposited on a softer substrate. We have shown that the Bückle's rule does not apply, and therefore very thick coatings are needed. This problem may be solved by a combination of the measurement of the compound hardness of the coating/substrate system as function of the applied load and nonlinear finite element modeling.

We briefly discuss also the measurement of elastic moduli, stress in the coatings, and tensile yield strength.

Acknowledgment We would like to thank the company SHM s.r.o. for the financial support of our work and the Department of Chemistry of the Technical University of Munich for providing us with the infrastructure needed for this work.

References

Abadias G, Guerin P (2008) *In situ* stress evolution during magnetron sputtering of transition metal nitride thin films. Appl Phys Lett 93:111908-1-3

Abadias G, Koutsokeras LE, Patsalas PA, Leroy W, Depla D, Zlotsi SV, Uglov VV (2011) In situ stress evolution during growth of transition metal nitride films and nanocomposites. In: Nanomaterials: applications & properties. Proceedings of the 1-st international conference, Crimea, 1:355–364

Abadias G, Koutsokeras LE, Siozios A, Patsalas P (2013) Stress, phase stability and oxidation resistance of ternary Ti–Me–N (Me = Zr, Ta) hard coatings. Thin Solid Films 538:56–70

Abadias G, Djema P, Belliard L (2014a) Alloying effects on the structure and elastic properties of hard coatings based on ternary transition metal (M = Ti, Zr or Ta) nitrides. Surf Coat Technol 257:129–137

Abadias G, Kanoun MB, Goumri-Said S, Koutsokeras L, Dub SN, Djemas P (2014b) Electronic structure and mechanical properties of ternary ZrTaN alloys studied by *ab initio* calculations and thin-film growth experiments. Phys Rev B 90:144107-1-18

Abadias G, Fillon A, Colin JJ, Michel A, Jaouen C (2014c) Real-time stress evolution during early growth stages of sputter-deposited metal films: influence of adatom mobility. Vacuum 100:36–40

Anderson TL (1995) Fracture mechanics, fundamentals and applications, 2nd edn. CRC Press, Boca Raton

Bayer RG (2002) Wear analysis for engineers. NHB Publishing, New York

Behncke H-H (1993) Bestimmung der Universalhärte und anderer Kennwerte an dünnen Schichten, insbesondere Hartstoffschichten. Härterei-Technische Mitteilungen 48:3–10

Berg G, Friedrich C, Broszeit E, Berger C (2000) Data collection of properties of hard materials. In: Riedel R (ed) Handbook of ceramic hard materials, vol 2. Wiley-VCH, Weinheim

Bolshakov A, Oliver WC, Pharr GM (1996) Influences of stress on the measurement of mechanical properties using nanoindentation: part II. Finite element simulations. J Mater Res 11:760–768

Bolshakov A, Pharr GM (1997) Inaccuracies in Sneddon's solution for elastic indentation by a rigid cone and their implications for nanoindentation data analysis. Mater Res Soc Symp Proc 436:189–194
Bolshakov A, Oliver WC, Pharr GM (1997) Finite element studies of the influence of pile-up on the analysis of nanoindentation data. Mat Res Soc Symp Proc 436:141–146
Bolshakov A, Pharr MG (1998) Influences of pileup on the measurement of mechanical properties by load and depth sensing indentation techniques. J Mater Res 13:1049–1058
Bouzakis K-D, Mirisidis I, Michailidis N, Lili N, Sampris A, Erkens G, Cremer R (2007) Wear of tools coated with various PVD films: correlation with impact test results by means of FEM simulations. Plasma Processes Polym 4:301–310
Brazhkin V, Dubrovinskaia N, Nicol M, Novikov N, Riedel R, Solozhenko V, Zhao Y (2004) What does 'harder than diamond' mean? Nat Mater 3:576–577
Bückle H (1965) Mikrohärteprüfung und ihre Anwendungen, Berliner Union, Waiblinger Kreiszeitung, Stuttgart 1965. German translation from L'Essai de Microdurete et ses Applications, Publications Scientific et Techniques du Ministère de L'Air, 1960
Bückle H (1973) In: Westbrook JH, Conrad H (eds) The science of hardness testing and its research applications. American Society for Metals, Metals Park, Ohio, pp 453–494
Bull SJ, Berasetegui EG, Page TF (2004) Modelling of indentation response of coatings and surface treatments. Wear 256:857–866
Chang YY, Jacobsen SD, Kimura M, Irifune T, Ohno I (2014) Elastic properties of transparent nano-polycrystalline diamond measured by GHz-ultrasonic interferometry and resonant sphere methods. Phys Earth Planet In 228:47–55
Chason E (2012) A kinetic analysis of residual stress evolution in polycrystalline thin films. Thin Solid Films 526:1–14
Chaudhri MM (2001) A note on a common mistake in the analysis of nanoindentation data. J Mater Res 16:336–339
Chaudhri MM, Lim YY (2007) Nanoindentation techniques: a critical assessment of the current methods of data analysis. Key Eng Mater 345–346:1107–1114
Chudoba T, Jennett NM (2008) Higher accuracy analysis of instrumented indentation data obtained with pointed indenters. J Phys D Appl Phys 41:215407-1-16
Chung H-Y, Weinberger MB, Levine JB, Kavner A, Yang J-M, Tolbert SH, Kaner RB (2007) Synthesis of ultra-incompressible superhard rhenium diboride at ambient pressure. Science 316:436–439
Cynn H, Klepeis JE, Yoo CS, Young DA (2002) Osmium has the lowest experimentally determined compressibility. Phys Rev Lett 88:135701-1-4
Doerner MF, Nix WD (1986) A method for interpreting the data from depth-sensing indentation instrument. J Mater Res 1:601–609
Dub SN, Brazhkin VV, Belous VA, Tolmacheva GN, Konevskii PV (2014) Comparative nanoindentation of single crystals of hard and superhard oxides. J Superhard Mater 36:217–230
Eremets MI, Trojan IA, Gwaze P, Huth J, Boehler R, Blank VD (2005) The strength of diamond. Appl Phys Lett 87:141902-1-3
Feynman RP, Leighton RB, Sands M (1966) The Feynman lectures on physics, I. Addison-Wesley, Reading, p 12-3-5
Fillon A, Abadias G, Michel A, Jaouen C, Villechaise P (2010) Influence of phase transformation on stress evolution during growth of metal thin films on silicon. Phys Rev Lett 104:096101-1-4
Fischer-Cripps AC (2004) Nanoindentation, 2nd edn. Springer, New York
Fischer-Cripps AC, Karvankova P, Veprek S (2006) On the measurement of hardness of superhard coatings. Surf Coat Technol 200:5645–5654
Fischer-Cripps AC, Bull SJ, Schwarzer N (2012) Critical review of claims for ultra-hardness in nanocomposite coatings. Philos Mag 92:1601–1630
Gottstein G (2004) Physical foundations of material science. Springer, Berlin
Gogotsi YG, Kailer A, Nickel KG (1999) Transformation of diamond to graphite. Nature 401:663–664

Gouldstone A, VanVliet KJ, Suresh S (2001) Simulation of defect nucleation in a crystal. Nature 411:656
Hall WH (1949) X-ray line broadening in metals. Proc Phys Soc (Lond) A 62:741–743
Hall WH, Williamson GK (1951) The diffraction pattern of cold worked metals: I the nature of extinction. Proc Phys Soc 64(B):937–946
Hay JC, Bolshakov A, Pharr GM (1999) A critical examination of the fundamental relations used in the analysis of nanoindentation data. J Mater Res 14:2296–2305
He JL, Veprek S (2003) Finite element modeling of indentation into superhard coatings. Surf Coat Technol 163–164:374–379
Hertzberg RW (1989) Deformation and fracture mechanics of engineering materials, 3rd edn. John Wiley, New York
Hill R (1950) The mathematical theory of plasticity. Oxford University Press, Oxford
Holleck H (1986) Material selection for hard coatings. J Vac Sci Technol A 4:2661–2669
Huang Q, Yu D, Xu B, Hu W, Ma Y, Wang Y, Zhao Z, Wen B, He J, Liu Z, Tian Y (2014) Nanotwinned diamond with unprecedented hardness and stability. Nature 510:250–253
Inspektor A, Salvador PA (2014) Architecture of PVD coatings for metalcutting applications: a review. Surf Coat Technol 257:138–153
Ivashchenko VI, Veprek S, Argon AS, Turchi PEA, Gorb L, Hill F, Leszczynski J (2015) First-principles quantum molecular calculations of structural and mechanical properties of TiN/SiNx heterostructures, and the achievable hardness of the nc-TiN/SiNx nanocomposites. Thin Solid Films 578:83–92
Jacobsen SD, Reichmann HJ, Kantor A, Spetzler HA (2005) A gigahertz ultrasonic interferometer for the diamond anvil cell and high-pressure elasticity of some iron-oxide minerals. In: Chen A, Wang Y, Duffy TS, Shen G, Dobrzhinetskaya LF (eds) Advances in high-pressure technology for geophysical applications. Elsevier, Amsterdam, pp 25–48
Janssen GCAM, Abdalla MM, van Keulen F, Pujada BR, van Venrooy B (2009) Celebrating the 100th anniversary of the Stoney equation for film stress: developments from polycrystalline steel strips to single crystal silicon wafers. Thin Solid Films 517:1858–1867
Jayaraman A (1983) Diamond anvil cell and high-pressure physical investigations. Rev Mod Phys 55:65–108
Johnsson B, Hogmark S (1984) Hardness measurements of thin films. Thin Solid Films 114:257–269
Karvankova P, Männling HD, Eggs C, Veprek S (2001) Thermal stability of ZrN–Ni and CrN–Ni superhard nanocomposite coatings. Surf Coat Technol 146–147:280–285
Kelly A, Macmillan NH (1986) Strong solids, 3rd edn. Clarendon, Oxford
Keutenedjian Mady CE, Rodriguez SA, Gomez AG, Souza RM (2012) Numerical analysis of different methods to calculate residual stresses in thin films based on instrumental indentation data. J Mater Res 27:1732–1741
Klug HP, Alexander LE (1974) X-ray diffraction procedures for polycrystalline and amorphous materials, 2nd edn. John Wiley, New York
Knotek O, Bosserhoff B, Schrey A, Leyendecker T, Lemmer O, Esser S (1992) A new technique for testing the impact load of thin films: the coating impact test. Surf Coat Technol 54/55:102–107
Kollenberg W (1988) Plastic deformation of Al_2O_3 single crystals by indentation at temperatures up to 750 °C. J Mater Sci 23(1988):3321–3325
Korsunsky AM, McGurk MR, Bull SJ, Page TF (1998) On the hardness of coated systems. Surf Coat Technol 99:171–183
Kyocera (2015) company, Kyoto Japan: http://global.kyocera.com/prdct/fc/product/pdf/s_c_sapphire.pdf downloaded 2015
Li J, VanVliet KJ, Zhu T, Yip S, Suresh S (2002) Atomistic mechanism governing elastic limit and incipient plasticity in crystals. Nature 418:307–310
Li ZS, Fang QF, Veprek S, Li SZ (2004) Evaluation of the internal friction and elastic modulus of the superhard films. Mater Sci Eng A 370:186–190

Li SZ, Fang QF, Liu Q, Li ZS, Gao J, Nesladek P, Prochazka J, Veprek-Heijman MGJ, Veprek S (2005) Thermally activated relaxation processes in superhard nc-TiN/a-Si_3N_4 and nc-$(Ti_{1-x}Al_x)$N/a-Si_3N_4 nanocomposites studied by means of internal friction measurements. Compos Sci Technol 65:735–774

Mayrhofer PH, Mitterer C, Hultman L, Clemens H (2006) Microstructural design of hard coatings. Prog Mater Sci 51:1032–1114

McClintock FA, Argon SA (1966) Mechanical behavior of materials. Addison-Wesley, Reading

Meyer E (1908) Untersuchungen über Härteprüfung und Härte. Zt Vereins Deutsch Ing 53:645–654

Meza JM, More Farias MC, De Souza RM, Cruz Riano LJ (2007) Using the ratio: maximum load over unload stiffness squared, P_m/S_u. On the evaluation of machine stiffness and area function of blunt indenters on depth-sensing indentation equipment. J Mater Res 10:437–447

Mittemeijer EJ, Welzel U (2008) The "State of the Art" of the diffraction analysis of crystallite size and strain. Z Krist 223:552–560

Müller B, Grau P, Kluge G (1984) The hardness of chromium- and titanium-doped sapphire crystals. Phys Status Solidi 83:499–506

Musil J (2000) Hard and superhard nanocomposite coatings. Surf Coat Technol 125:322–330

Musil J, Kadlec S, Vyskocil J, Valvoda V (1988) New results in D.C. Reactive magnetron deposition of TiN films. Thin Solid Films 167:107–119

Niederhofer A, Nesladek P, Männling HD, Moto K, Veprek S, Jilek M (1999) Structural properties, internal stress and thermal stability of nc-TiN/a-Si_3N_4, nc-TiN/$TiSi_x$ and nc-$(Ti_{1-y}Al_ySi_x)$N superhard nanocomposite coatings reaching the hardness of diamond. Surf Coat Technol 120–121:173–178

Noyan IC, Cohen JB (1987) Residual stress measurement by diffraction and interpretation. Springer, New York

Oliver WC, Pharr GM (1992) An improved technique for determining hardness and elastic modulus using load and displacement sensing indentation experiment. J Mater Res 7:1564–1583

Oliver WC, Pharr GM (2004) Measurement of hardness and elastic modulus by instrumented indentation: advances in understanding and refinements to methodology. J Mater Res 19:3–20

Pelleg J, Elish E, Mogilyanski D (2005) Evaluation of average domain size and microstrain in a silicide film by the Williamson–Hall method. Metall Mater Trans A 36:3187–3194

Pharr GM, Herbert EG, Gao Y (2010) The indentation size effect: a critical examination of experimental observations and mechanistic interpretations. Annu Rev Mater Res 40:271–292

Rodrigez SA, Souza RM, Alcala J (2011) A critical assessment of elastic unloading in sharp instrumented indentation experiments and the extraction of mechanical properties. Philos Mag 91:1409–1423

Rose JH, Smith AR, Guinea F, Ferrante J (1984) Universal features of the equation of state of metals. Phys Rev B 29:2963–2969

Sinani AB, Dynkin NK, Konevskiy PV, Lytvynov LA (2009) Dependence of sapphire hardness on loading type and orientation. Bull Russ Acad Sci Phys 73:456–459

Stoney GG (1909) The tension of metallic films deposited by electrolysis. Proc R Soc Lond A 82:172–175

Sun Y, Bell T, Zheng S (1995a) Finite element analysis of the critical ratio of coating thickness to indentation depth for coating property nanoindentation measurements. Thin Solid Films 258:198–204

Sun Y, Bloyce A, Bell T (1995b) Finite element analysis of plastic deformation of various TiN coating-substrate systems under normal contact with a rigid sphere. Thin Solid Films 271:122–131

Tabor D (1951) The hardness of metals. At the Clarendon Press, Oxford

Taljat B, Zacharia T, Pharr GM (1998) Pile-Up behavior of spherical indentations in engineering materials. Mater Res Soc Symp Proc 522:33–38

Tian Y, Xu B, Yu D, Ma Y, Wang Y, Hang Y, Hu W, Tang C, Gao Y, Luo K, Zhao Z, Wang LM, Weng B, He J, Liu Z (2013) Ultrahard nanotwinned cubic boron nitride. Nature 493:385–388

Tsui TY, Oliver WC, Pharr GM (1996) Influence of stress on the measurement of mechanical properties using nanoindentation: part I. Experimental studies in an aluminum alloy. J Mater Res 11:752–759

VanVliet KJ, Suresh S (2002) Simulation of cyclic normal indentation of crystal surfaces using the bubble-raft model. Philos Mag 82:1993–2001

Veprek RG, Parks DM, Argon AS, Veprek S (2007) Non-linear finite element constitutive modeling of mechanical properties of hard and superhard materials studied by indentation. Mater Sci Eng A 448:366–378

Veprek S, Sarott FA, Iqbal Z (1987) Effect of grain boundaries in the Raman spectra, optical absorption, and elastic light scattering in nanometer-sized crystalline silicon. Phys Rev B 36:3344–3350

Veprek S, Reiprich S (1995) A concept for the design of novel superhard coatings. Thin Solid Films 268:64–71

Veprek S, Haussmann M, Reiprich S (1996) Superhard nanocrystalline W_2N/amorphous Si_3N_4 composite materials. J Vac Sci Technol A 14:46–51

Veprek S (1999) The search for novel, superhard materials. J Vac Sci Technol A 17:2401–2420

Veprek S, Argon AS (2002) Towards the understanding of mechanical properties of super- and ultrahard nanocomposites. J Vac Sci Technol B 20:650–664

Veprek S, Mukherjee S, Karvankova P, Männling H-D, He JL, Moto K, Prochazka J, Argon AS (2003a) Hertzian analysis of the self-consistency and reliability of the indentation hardness measurements on superhard nanocomposite coatings. Thin Solid Films 436:220–231

Veprek S, Mukherjee S, Karvankova P, Männling H-D, He JL, Moto K, Prochazka J, Argon AS (2003b) Limits to the strength of super- and ultrahard nanocomposite coatings. J Vac Sci Technol A 21:532–544

Veprek S, Mukherjee S, Karvankova P, Männling H-D, He JL, Xu J, Prochazka J, Argon AS, Li AS, Fang QF, Li SZ, Manghnani MH, Tkachev S, Zinin P (2003c) Possible artefacts in the measurement of hardness and elastic modulus on superhard coatings and the verification of the correctness of the data. Mater Res Soc Symp Proc 750:9–15

Veprek S, Veprek-Heijman MGJ, Karvankova P, Prochazka J (2005) Different approaches to superhard coatings and nanocomposites. Thin Solid Films 476:1–29

Veprek S, Veprek-Heijman MGJ (2008) Industrial applications of superhard nanocomposite coatings. Surf Coat Technol 202:5063–5073

Veprek S, Argon AS, Zhang RF (2010a) Design of ultrahard materials: Go nano! Philos Mag 90:4101–4115

Veprek S, Prilliman SG, Clark AM (2010b) Elastic moduli of nc-TiN/a-Si_3N_4 nanocomposites: compressible, yet superhard. J Phys Chem Solids 71:1175–1178

Veprek S (2013) The search for new superhard materials: Go nano! J Vac Sci Technol A 31:050822-1-33

Veprek-Heijman MGJ, Veprek RG, Argon AS, Parks DM, Veprek S (2009) Non-linear finite element constitutive modeling of indentation into super- and ultrahard materials: the plastic deformation of the diamond tip and the ratio of hardness to tensile yield strength of super- and ultrahard nanocomposites. Surf Coat Technol 203:3385–3391

Veprek S, Veprek-Heijman MGJ (2012) Limits to the preparation of superhard nanocomposites: impurities, deposition and annealing temperature. Thin Solid Films 522:274–282

Veprek-Heijman MGJ, Veprek S (2015) The deformation of the substrate during indentation into superhard coatings: Bückle's rule revised. Surf Coat Technol 284:206–214

Warren BE, Averbach BL (1952) The separation of cold-work distortion and particle size broadening in X-Ray patterns. J Appl Phys 23:497–498

Williamson GK, Hall WH (1953) X-ray line broadening from filed aluminium and wolfram. Acta Metall 1:22–31

Xu B, Tian Y (2015) Ultrahardness: measurement and enhancement. J Phys Chem C 119:5633–5638

Zhang RF, Legut D, Niewa R, Argon AS, Veprek S (2010) Shear-induced structural transformation and plasticity in ultraincompressible ReB2 limit its hardness. Phys Rev B 82:104104-1-7

Zhang RF, Legut D, Wen XD, Veprek S, Rajan K, Lookman T, Mao HK, Zhao YS (2014) Bond deformation paths and electronic instabilities of ultraincompressible transition metal diborides: case study of OsB_2 and IrB_2. Phys Rev B 90:094115-1-6

Zhang XD, Meng WJ, Wang W, Rehn LE, Baldo PM, Evans RD (2004) Temperature dependence of structure and mechanical properties of Ti-Si-N coatings. Surf Coat Technol 177 (178):325–333

Zhu T, Li J, Ogata S, Yip S (2008) Mechanics of ultra-strength materials. MRS Bull 34:167–172

Zinin P, Manghnani MH, Tkacev S, Askarpour V, Lefeuvre O, Every A (1999) Brillouin spectroscopy of surface modes in thin-film Si_3N_4 on GaAs. Phys Rev B 60:2844–2850